Reverse Exponential Decay of Electrical Transmission in Nanosized Graphite Sheets

Tomofumi Tada and Kazunari Yoshizawa*

Institute for Materials Chemistry and Engineering, Kyushu University, Fukuoka 812-8581, Japan

Received: September 23, 2003; In Final Form: April 7, 2004

Quantum transport effects in a molecular junction composed of a nanosized graphite sheet and two gold leads are studied on the basis of Landauer's formalism. The formulation for tunneling current by Caroli, Combescot, Nozieres, and Saint-James is extended to incorporate multiple interactions in a metal−insulator connecting region. A large variation of conductance is obtained, depending on the manner of connections between a graphite sheet and two gold chains. Connections between zigzag-edge sites and gold chains have significant transport effects. Graphite sheets of several sizes are studied to increase our understanding of the exponential law of conductance $g = g_0 e^{-\gamma L}$, in which L is the molecular length and γ is the damping factor. Reverse exponential law with negative γ is observed in graphite sheets with zigzag edges. That is, the conductance is enhanced with an increase in L. This interesting behavior of conductance is due to the unique nature of the HOMO and LUMO localized in the zigzag-edge regions and the remarkable decrease in the HOMO−LUMO gap with L. Quantum transport effects in graphite sheets with defects such as a disordered zigzag edge are also studied. It is found that the regular zigzag-edge structures lead to effective quantum transport in graphite sheets.

Introduction

Electrical transmission through molecular junctions consisting of single molecules is an important issue in the development of molecular electronics in nanotechnology. Landauer's formalism[1,2] using a Green's function method is of great use in calculating the conductance of molecular wires at the single molecule level, e.g., benzen-1,4-dithiol,[3−8] fullerene C_{60},[9−11] and tape-porphyrin oligomers.[12] Sophisticated algorithms based on the formalism combined with density functional theory (DFT)[13,14] were recently proposed.[15−17] In the fundamental understanding of electrical transmission in molecular wires, issues of adsorption of molecules on electrodes, heteroatomic effects, and correlation between molecular length L and conductance are important. The exponential law of conductance $g = g_0 e^{-\gamma L}$ is useful to characterize molecular wires. Magoga and Joachim calculated the damping factor γ in several conjugated oligomers;[18] for example, γ's of the poly(acetylene) and poly(*para*-phenylene) oligomers shown in Chart 1 are 0.187 and 0.281 Å^{-1}, respectively. The conductance therefore decreases with an increase in L. They also showed that good contact conductance g_0 is obtained by optimizing the molecular wire end.

Quantum transport effects in nanosized systems correlate with the electronic states of molecules incorporated into molecular junctions. In a previous paper, we derived an interesting relationship between frontier molecular orbitals (MOs) and conductance within Landauer's formalism.[19] We also studied heteroatomic effects on the conductance of nanosized graphite sheets.[20] Since heteroatoms can localize the electronic population in the highest occupied MO (HOMO) and the lowest unoccupied MO (LUMO), quantum transport is significantly enhanced by heteroatoms. In the present paper, we derive a formulation for conductance by extending the one-dimensional model developed by Caroli, Combescot, Nozieres, and Saint-James (CCNS)[21] and present quantum transport effects in a molecular junction composed of a nanosized graphite sheet and two gold chains (chain−molecule−chain junction), in which we used a linear gold chain as a metallic lead. We used the B3LYP[22] DFT method and the Pariser−Parr−Pople (PPP) method[23] in this study. The molecular junctions adopted in this study are not unrealistic because multi-shell gold nanowires[24] and one-dimensional gold chains[25] are available at present. We pay special attention to the exponential law of conductance and influences caused by defects in graphite sheets.

CHART 1

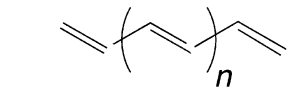

poly(acetylene)

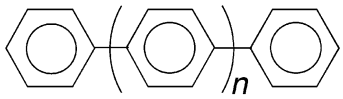

poly(*para*-phenylene)

Method of Calculation

Extended CCNS Formulation. The formulation for tunneling current by CCNS[21] provides a practical procedure for calculating electrical conductance on the basis of Landauer's formalism. The system used in the CCNS formulation is a linear metal−insulator−metal (MIM) junction, in which the perturbation leading to electrical transmission is represented by a single interaction between M and I. To take multiple interactions into account, we extended the CCNS formulation to a general one. Figure 1a shows a schematic representation of a molecular junction composed of two linear gold chains and a molecule.

* To whom correspondence should be addressed. E-mail: kazunari@ms.ifoc.kyushu-u.ac.jp.

10.1021/jp0310908 CCC: $27.50
Published on Web 05/18/2004

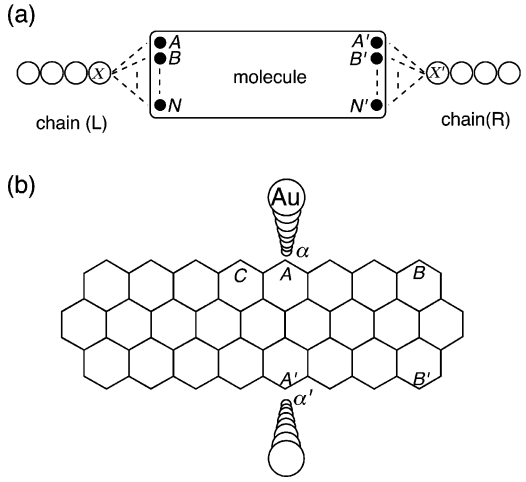

Figure 1. (a) Schematic representation of a chain-molecule-chain junction. (b) Molecular junction composed of $C_{72}H_{24}$ and two gold chains.

Points A, B, ..., N (A′, B′, ..., N′) mean atoms in the left (right) side of a molecule, and X (X′) means a terminal gold atom in the left (right) chain. The interactions between two atoms (e.g., A and X) are represented in terms of several integrals based on atomic orbitals (AOs), e.g., the 2pπ AO in carbon and the 6s AO in gold. Here we use indices a, b, c, ... (a′, b′, c′, ...) as the AOs in the left (right) side of a molecule. Let us consider Green's functions between two AOs in a molecule. The Dyson equation for $G_{ij'}$ is written as

$$G_{ij'} = G_{ij'}^{(0)} + \sum_r \sum_s G_{ir}^{(0)} \tau_{rs} G_{sj'} + \sum_{r'} \sum_{s'} G_{ir'}^{(0)} \tau_{r's'} G_{s'j'} \quad (1)$$

$$\tau_{rs} = \beta_{r\alpha}^{T} G_{\alpha\alpha}^{(0)} \beta_{\alpha s}^{T} \quad (2)$$

and

$$\tau_{r's'} = \beta_{r'\alpha'}^{T} G_{\alpha'\alpha'}^{(0)} \beta_{\alpha's'}^{T} \quad (3)$$

where $G^{(0)}$ is the 0-th order Green's function, and $\beta_{r\alpha}^{T}$ is the transfer integral between the rth AO in a molecule and the αth AO in a gold chain. The 0th order Green's function $G^{(0)}$ can be calculated by neglecting the interactions between the three subsystems: the molecule and the two gold chains. The α (α') identifies the 6s AO of the terminal gold atom in the left (right) chain. Although we considered only the 6s AOs of the terminal gold atoms in gold chains, this assumption is reasonable from DFT calculations of a one-dimensional gold chain, as described later in the Results and Discussion part. The Dyson equations for $G_{sj'}$ and $G_{s'j'}$ are written like in eq 1, and the Green's function $G_{ij'}$ is rewritten in terms of $G^{(0)}$'s and τ's by substituting the Dyson equations of $G_{sj'}$ and $G_{s'j'}$. Although it is difficult to carry out this procedure in a straightforward way, we obtained a useful expression for Green's function by extending the CCNS formulation step by step; see Appendix A. We finally obtained Green's function $G_{ij'}$ as follows:

$$G_{ij'} = \left[G_{ij'}^{(0)} \left(1 - \sum_{k(\neq i)} \sum_{l} G_{kl}^{(0)} \tau_{lk} - \sum_{k'(\neq j')} \sum_{l'} G_{k'l'}^{(0)} \tau_{l'k'} \right) + \sum_{m(\neq i)} \sum_{n} G_{im}^{(0)} \tau_{mn} G_{nj'}^{(0)} + \sum_{m'(\neq j')} \sum_{n'} G_{im'}^{(0)} \tau_{m'n'} G_{n'j'}^{(0)} \right] / D \quad (4)$$

and

$$D = \prod_k (1 - \sum_l G_{kl}^{(0)} \tau_{lk}) \prod_{k'} (1 - \sum_{l'} G_{k'l'}^{(0)} \tau_{l'k'}) - \sum_{k''(<l'')} \sum_{l''} \times (\dot{\sum_p} G_{k''p}^{(0)} \tau_{pl''}) (\dot{\sum_q} G_{l''q}^{(0)} \tau_{qk''}) \quad (5)$$

where indices k, l, m, and n (k', l', m', and n') cover the AOs in the left (right) side of a molecule, and indices k'' and l'' cover all of the AOs in the left and right sides of a molecule. The summations in the dotted Σ's are restricted as follows: when index l'' is one of the left (right) side AOs, the summation with p is restricted to the left (right) side AOs, and when index k'' is one of the left (right) side AOs, the summation with q is restricted to the left (right) side AOs. We derived this expression for Green's functions assuming that the self-energies τ s are smaller than 1 eV, as is satisfied for weak interactions such as van der Waals interactions.

Conductance g of a molecular junction in the zero temperature limit is related to the transmission coefficient $T(E)$ at the Fermi level E_F as follows:

$$g = \frac{2e^2}{h} T(E_F) \quad (6)$$

where $T(E)$ is given by

$$T(E) = \mathrm{Tr}[\mathbf{\Gamma G^R \Gamma G^A}] \quad (7)$$

The matrix elements of $\Gamma_{\mathbf{L}}$ and $\Gamma_{\mathbf{R}}$ are proportional to the local density of states (LDOS) ρ of gold atoms in the left and right leads, respectively, and are written as

$$(\Gamma)_{tu} = 2\pi \rho_\omega \beta_{t\alpha}^{T} \beta u_\alpha^{T} \quad (8)$$

and

$$(\Gamma)_{t'u'} = 2\pi \rho_\alpha{}' \beta_{t'\alpha'}^{T} \beta_{\alpha'u'}^{T} \quad (9)$$

The matrix elements of $\mathbf{G^R}$ ($\mathbf{G^A}$) are retarded (advanced) Green's functions, which are obtained by substituting $G^{(0)R}$ ($G^{(0)A}$) for $G^{(0)}$ in eqs 4 and 5. The quantity $G^{(0)R}$ ($G^{(0)A}$) is written in terms of MO coefficients C's and orbital energies ϵ's as follows:

$$G_{rs}{}^{(0)R/A}(E) = \sum_k \frac{C_{rk} C_{sk}^*}{E - \epsilon_k \pm i\eta} \quad (10)$$

The following equation that describes the relationship between the LDOS and the 0th order Green's function determines parameter η in eq 10:

$$\rho_j(E) = -\frac{1}{\pi} \mathrm{Im}\, G_{jj}^{(0)R}(E) \quad (11)$$

The MO coefficients and the orbital energies are obtained by solving the Hartree−Fock or Kohn−Sham equation. The methods of choice in calculating the 0th order Green's functions are the PPP method and the DFT at the B3LYP level of theory with the 6-31G[26] basis set. Details of the PPP method are described in Appendix B. The Gaussian 98 program[27] was used for the B3LYP calculations. In the connecting region between gold chains and a molecule, the integrals used are $\beta_{2p\pi-6s}^{T}$ = 0.4 eV[28] in the PPP method and $\beta_{2p\pi(I)-6s}^{T}$ = 0.2 eV and

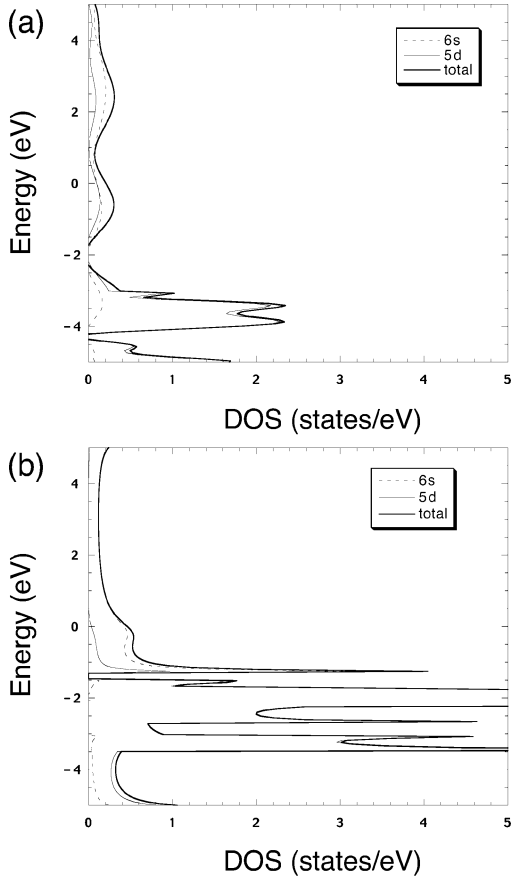

Figure 2. The total DOS and projected DOS of a gold atom in (a) bulk and (b) a linear chain. The Fermi level is set to be 0 eV.

$\beta^{T}_{2p\pi(O)-6s} = 0.2$ eV in the B3LYP method; 2pπ(I) and 2pπ(O) mean inner and outer 2pπ AOs, respectively.

Results and Discussion

LDOS of a Linear Gold Chain. To obtain the LDOS of a gold atom in a linear chain, we performed DFT calculations of periodic systems at the B3LYP level with quasirelativistic pseudopotentials introduced by Andrae and co-workers[29] using the CRYSTAL package.[30−32] We assumed the Au−Au distances in a linear chain to be 2.88 Å, which is equal to the separation between the nearest neighbor atoms in bulk gold. Figure 2 shows calculated DOS of a gold atom in bulk and the linear chain. In bulk gold, the contribution from the 6s orbital is comparable to that from the 5d orbitals at the Fermi level because the total DOS and the 6s- and 5d-projected DOS (6s-DOS and 5d-DOS) are 0.200, 0.098, and 0.094 states/eV, respectively. On the other hand, the total DOS at the Fermi level in the linear chain mainly derives from the 6s-DOS because the total DOS, 6s-DOS, and 5d-DOS are 0.462, 0.422, and 0.035 states/eV, respectively. Thus, we used the 6s-DOS as the LDOS of a gold atom in the linear chains.

Quantum Transport in $C_{72}H_{24}$. Let us consider a molecular junction composed of a nanosized graphite sheet and two gold chains. Figure 1b shows a schematic representation of the molecular junction in which two gold chains are aligned perpendicularly to the molecular plane of molecular graphite $C_{72}H_{24}$. This kind of graphite is now available since analogous graphitic molecules were synthesized from photocyclization and dehydrogenation.[33] Figure 3 shows transmission coefficients calculated from the extended CCNS formulation within the B3LYP and the PPP methods assuming that the Fermi level is

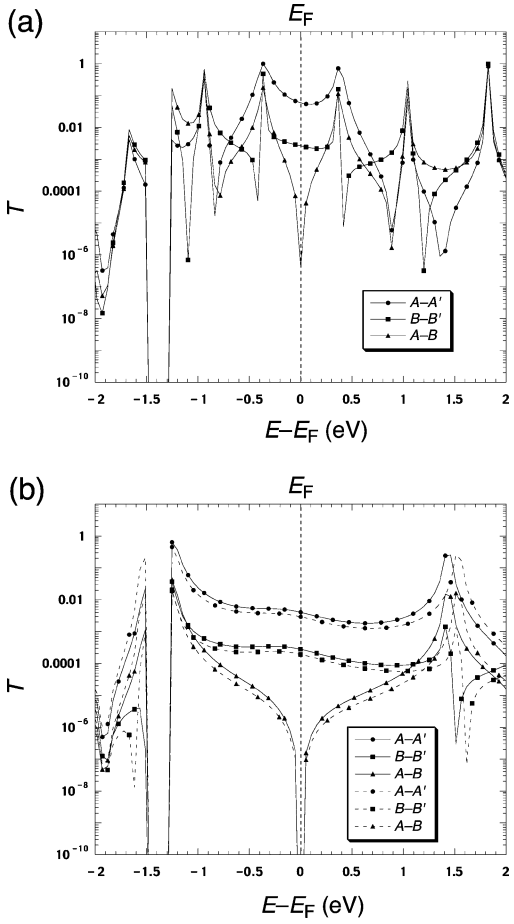

Figure 3. Computed transmission coefficients in $C_{72}H_{24}$ at the (a) the B3LYP/6-31G and (b) the PPP levels of theory. The dotted and solid lines in (b) are respectively transmission coefficients in an optimized geometry and those in a nonoptimized geometry, in which the C−C bond lengths are 1.4 Å, the C−H bond lengths are 1.1 Å, and all of the bond angles are 120°.

located at the midgap of the graphite sheet. We used a geometry of $C_{72}H_{24}$ optimized at the B3LYP/6-31G level of theory. Calculated T's are sharp near the orbital energies ϵ's of $C_{72}H_{24}$ because the 0th order Green's function increases near these energies (see eq 10). The peaks at −0.4 eV and +0.4 eV obtained from the B3LYP calculations (Figure 3a) originate from the HOMO and LUMO, respectively, and the peaks at +1.5 eV obtained from the PPP calculations (Figure 3b) come from the LUMO. Since the LDOS of gold in the linear chain is zero near −1.5 eV (see Figure 2b), the transmission coefficients around −1.5 eV are zero. If the LDOS of gold in the linear chain is not zero near −1.5 eV, the peaks coming from the HOMO will be obtained at −1.5 eV in the PPP calculations. Chart 2 shows the HOMO and LUMO of $C_{72}H_{24}$ at the B3LYP/6-31G level, in which the size of each circle corresponds to the population of 2pπ AO and the solid and open circles show the sign of MO coefficient C. The HOMOs and LUMOs calculated with the B3LYP/6-31G and the PPP methods are essentially identical.

As shown in Figure 3, transmission coefficients obtained by connecting the linear gold chains with atoms A and A′ ($T_{AA'}$'s) are large, but $T_{BB'}$'s and T_{AB}'s are small at the Fermi level. Thus, the conductance of the molecular junction significantly depends on the manner of connections between the gold chains and the graphite sheet. The variation of T's is well characterized by looking at the correlations between the frontier orbitals and the conductance. The largest transmission coefficient $T_{AA'}$ at

CHART 2

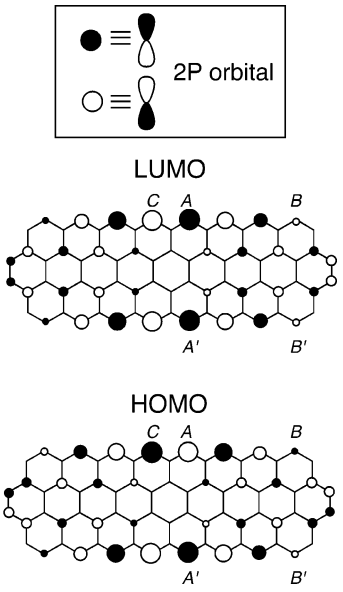

the Fermi level is in line with the statement that two atoms with large MO coefficients in the HOMO and LUMO should be connected with metallic leads to obtain effective quantum transport.[19,20] Thus, the formulation derived in this study provides reasonable results with respect to the electrical transmission in nanosized graphite sheets. Although the HOMO−LUMO energy gap obtained from the B3LYP calculation (0.74 eV) is different from that of the PPP calculation (3.06 eV), the general features ($T_{AA'}(E_F) > T_{BB'}(E_F) > T_{AB}(E_F)$) are identical. So, we mainly used the PPP method in the calculations of quantum transport effects in nanosized graphite sheets.

How we define the Fermi level of molecular systems is a difficult problem in the calculations of conductance, but the definition of the reasonable position has not yet been established. The Fermi level of carbon nanotubes is observed to shift from the midgap toward the HOMO by 0.3 eV.[34,35] Thus, we considered how the Fermi-level shift ΔE_F toward the HOMO can change the transmission coefficients. Figure 4 shows T_{AB}'s with $\Delta E_F = 0.0 \sim 0.3$ eV within the PPP framework. The transmission coefficient T_{AB} at the Fermi level increases with an increase in ΔE_F, and those in other connections also increase with ΔE_F because the resonance of transmission coefficients takes place at MO energies. Table 1 lists transmission coefficients $T_{AA'}$, $T_{BB'}$, T_{AB}, and T_{AC} with several ΔE_F values. Transmission $T_{AA'}(E_F)$ is the largest even if the Fermi level is shifted up to 0.3 eV. When the Fermi level is located at the midgap ($\Delta E_F = 0$), $T_{AA'}$ and T_{AC} show quite different transmissions despite identical populations of 2pπ AOs at atoms A, A′, and *C*. This result is fully consistent with the other statement that the product of MO expansion coefficients on the two atoms in the HOMO must be different in sign from that in the LUMO for effective quantum transport.[19] The conductance of molecular junctions correlates with the signs of MO coefficients as well as with the magnitude of MO coefficients, as described earlier.

Quantum Transport Effects in Small-Gap Systems. We considered quantum transport in several graphite sheets, the HOMO−LUMO energy gaps of which are different from that of $C_{72}H_{24}$. In Figure 5a, we represent the graphite sheets treated in this study as R($2n_x$,n_y). For example, the graphite sheet depicted in Figure 1b corresponds to R(8,3). Since the geometry optimization of nanosized graphite sheets does not lead to a significant change in the transmission coefficients at the Fermi level (see Figure 3b), here we assumed the C−C bond lengths

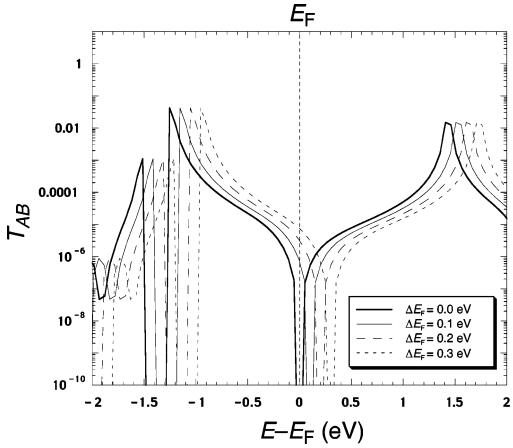

Figure 4. Transmission coefficients T_{AB}'s calculated with Fermi-level shifts, $\Delta E_F = 0.0$, 0.1, 0.2, and 0.3 eV.

TABLE 1: Transmission Coefficients at the Fermi Level in $C_{72}H_{24}$[a]

	$T(E_F)$ (10^{-4})			
ΔE_F (eV)	$T_{AA'}$	$T_{BB'}$	T_{AB}	T_{AC}
0.0	40.14	2.78	0.00	0.00
0.1	40.66	2.80	0.01	0.16
0.2	41.95	2.83	0.03	0.64
0.3	44.10	2.89	0.06	1.53

[a] A variation in the Fermi-level shift ΔE_F of up to 0.3 eV is considered.

to be 1.4 Å, the C−H bond lengths 1.1 Å and all of the bond angles 120°. Nanosized graphite sheets used are R(4,3), R(6,3), R(8,3), R(6,7), R(8,7), R(6,11), and R(8,11),[36] whose energy gaps obtained from the PPP method are 4.95, 3.58, 2.86, 1.99, 1.26, 1.06, and 0.69 eV, respectively. According to experimental studies, energy gaps of polynuclear aromatic hydrocarbons are larger than about 2.5 eV,[37] corresponding to the energy gaps of R(4,3), R(6,3), and R(8,3). Other graphite sheets, R(6,7), R(8,7), R(6,11), and R(8,11), are efficient to consider quantum transport effects in small-gap systems. We calculated three types of transmission coefficients $T_I(E_F)$, $T_{II}(E_F)$, and $T_{III}(E_F)$; connections in the calculations of T_I, T_{II}, and T_{III} are depicted in Figure 5b−d. For example, $T_{AA'}$, T_{AC}, and $T_{BB'}$ in R(8,3) correspond to T_I, T_{II}, and T_{III}, respectively. Figure 6 shows the three types of transmission coefficients in several nanosized graphite sheets when $\Delta E_F = 0.3$ eV. As expected from our earlier work,[19] $T_I(E_F)$ is the largest in the energy gap range 0.69−4.95 eV, and $T_{III}(E_F)$ is the smallest in the same energy range. However, in a system whose energy gap is smaller than 1 eV, $T_I(E_F)$ and $T_{II}(E_F)$ show the same order of magnitude for transmission. In such a small-gap system, the energy of the HOMO is close to the Fermi level, so the contribution from the HOMO dominates in eq 10. Consequently, the magnitude of MO coefficients in the HOMO correlates significantly with the electrical transmission in such a case, and therefore, T_{II} shows a large transmission comparable to T_I.

Reverse Exponential Decay of Conductance in Graphite Sheets. In general, the conductance of a molecular wire follows the exponential law $g = g_0 e^{-\gamma L}$ with the damping factor γ and the interlead separation L.[18] To look at this law in graphite sheets, we considered the R(8,n_y) series (R(8,3), R(8,7), R(8,11), R(8,15), and R(8,19)).[38] We also treated poly(acetylene) and poly(*para*-phenylene) oligomers shown in Chart 1 for comparison. In R(8,n_y), we computed transmission coefficients in the best connection (i.e., $T_I(E_F)$), and in poly(acetylene) and poly(*para*-phenylene), we made connections with metallic leads at

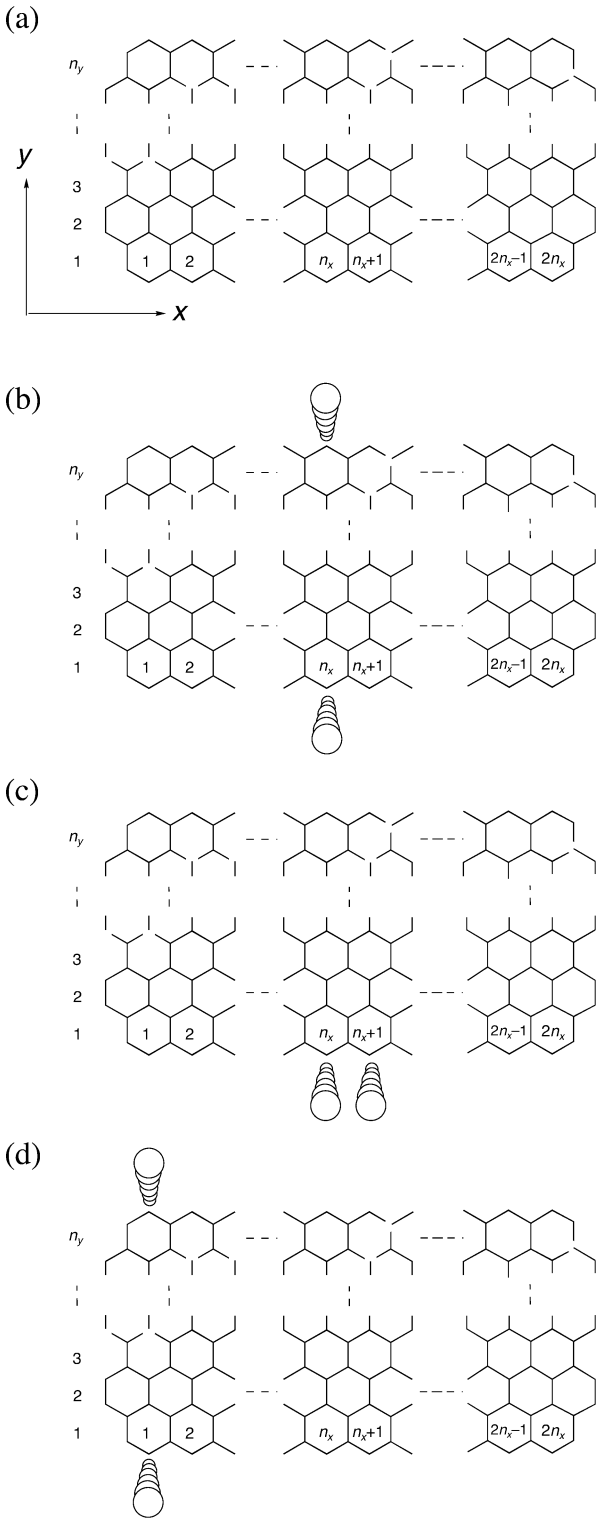

Figure 5. (a) Nanosized graphite sheets R($2n_x$,n_y). The three types of connections (b), (c), and (d) are used in the calculations of transmission coefficients T_{I}, T_{II}, and T_{III}, respectively.

the terminal carbon atoms. Since the Fermi-level shift is not essential for the estimation of γ, we assumed here the Fermi level to be located at the midgap.

Figure 7 shows calculated transmission coefficients in R(8,n_y), poly(acetylene), and poly(*para*-phenylene), and their HOMO−LUMO energy gaps. We estimated γ in the exponential law from Figure 7a. In poly(acetylene) and poly(*para*-phenylene), we observed the exponential decay of transmission coefficients with increasing L, being in good agreement with that obtained

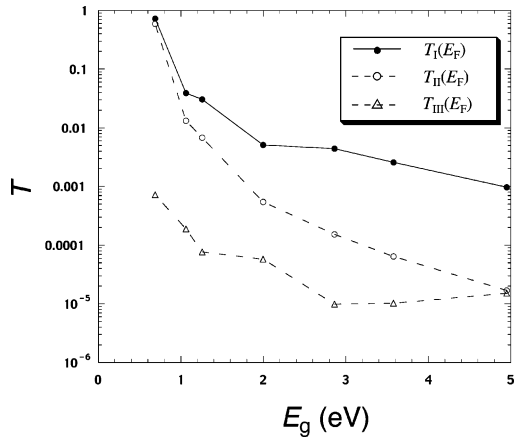

Figure 6. Computed transmission coefficients $T_{\mathrm{I}}(E_{\mathrm{F}})$, $T_{\mathrm{II}}(E_{\mathrm{F}})$, and $T_{\mathrm{III}}(E_{\mathrm{F}})$ vs energy gaps E_{g}. The Fermi-level shift ΔE_{F} was set to be 0.3 eV.

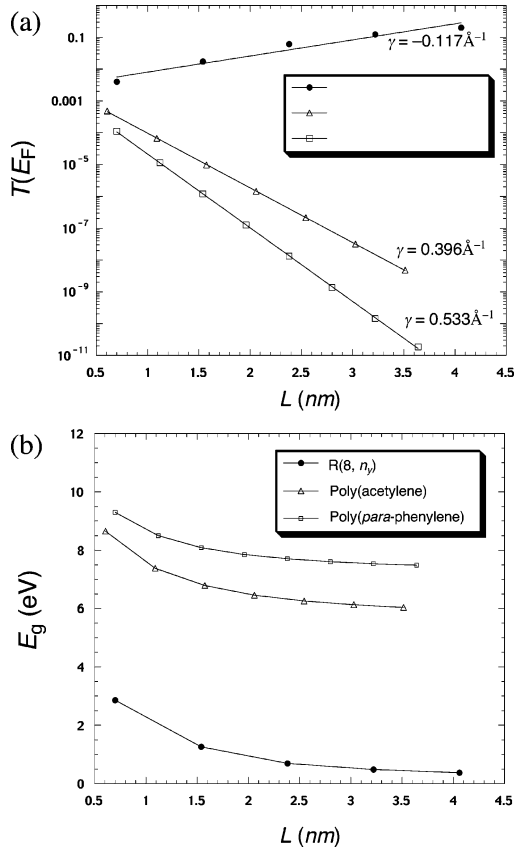

Figure 7. (a) Transmission coefficients in R(8,n_y), poly(acetylene), and poly(*para*-phenylene). L is the interlead separation. The Fermi level was set to be the midgap. (b) Energy gaps of R(8,n_y), poly(acetylene), and poly(*para*-phenylene).

by Magoga and Joachim.[18] However, the transmission coefficients in R(8,n_y) are enhanced with an increase in L. Although the energy gap decreases with L in a similar way in these systems, the electrical transmission in R(8,n_y) shows this surprising exponential law with negative γ. Clearly, the remarkable localization of orbital amplitude in the HOMOs and LUMOs is the origin of this interesting result. As shown in Chart 2, the amplitude of the HOMO and LUMO is localized well at the zigzag edges. Consequently, the numerators of Green's functions shown in eq 10 are nearly equal in magnitude in the R(8,n_y) series in the case of the good connections shown in Figure 5b. Since the energy gap decreases with increasing size of R(8,n_y), the denominator of the Green's function gets small.

CHART 3

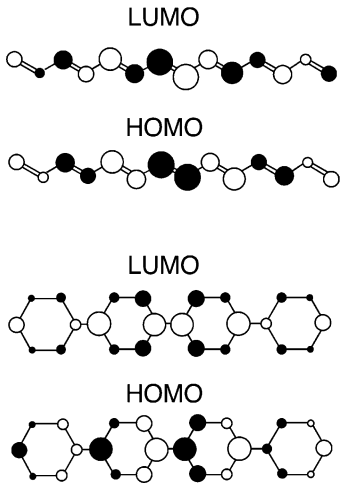

TABLE 2: Transmission Coefficients Computed from B3LYP/6-31G Calculations

graphite sheet	$T_I(E_F)$ (10^{-2})	E_g (eV)
R(8, 3)	5.88	0.74
R(8, 5)	15.95	0.40
R(8, 7)	42.70	0.24

TABLE 3: Largest Transmission Coefficient and the Energy Gap in Graphite Sheets

molecule	$T(E_F)$ (10^{-3})	E_g (eV)
R(8,7)	17.30	1.26
Z-disordered sheet	2.27	2.22
A-disordered sheet	22.56	1.11
holed sheet	26.72	1.17

Therefore, we have highly enhanced transmission coefficients in large systems. On the other hand, we do not see such an exponential increase of transmission coefficients in the poly(acetylene) and poly(*para*-phenylene) oligomers. Since the π-electronic populations in the two oligomers are delocalized over the molecules, as shown in Chart 3, the π-electronic populations at the terminal atoms decrease with an increase in L. Consequently, the conductance of the two oligomers obeys the normal exponential law.

To better characterize the electrical transmission with negative γ, we reconsidered the reverse exponential devay of conductance at the B3LYP/6-31G level. Table 2 lists computed transmission coefficients $T_I(E_F)$ in R(8,3), R(8,5), and R(8,7).[39] We evaluated from Table 2 the damping factor γ in the exponential law and found negative γ (-0.234 Å^{-1}). The exponential increment of electrical transmission with an increase in L is also confirmed within the B3LYP/6-31G as well as the PPP frameworks.

Quantum Transport Effects in Graphite Sheets with Defects. To investigate a change in conductance by defects, we considered R(8,7) derivatives that involve disordered zigzag edges (abbreviated as Z-disordered sheet), disordered armchair edges (abbreviated as A-disordered sheet), and a hole (abbreviated as holed sheet), as shown in Figure 8. We are able to find effective sites for quantum transport by looking at the HOMOs and LUMOs in the molecular systems. Figure 8 shows the HOMOs and LUMOs of the graphite sheets, in which the red circles identify efficient sites for good quantum transport. The largest quantum transport in each graphite sheet is obtained by connecting these sites with metallic leads. Table 3 shows significant transmission coefficients and HOMO−LUMO gaps obtained within the PPP framework. In the Z-disordered sheet, as shown in Figure 8a, the defects in the zigzag edges result in the delocalization of π-electronic population in the HOMO and LUMO, and consequently, the magnitude of the quantum transport is decreased. On the other hand, the A-disordered sheet and the holed sheet retain localized π-electronic populations at the zigzag edges (see Figure 8, parts b and c) and exhibit slightly larger quantum transport than R(8,7). Since the magnitude of the localized population is not affected in the A-disordered sheet and the holed sheet, the decreased energy gaps in the two graphite sheets lead to the slightly enhanced quantum transport.

Conclusions

We have extended the formulation for tunneling current by CCNS to incorporate multiple interactions in a metal−insulator connecting region. We applied it in the calculations of the conductance of a molecular junction composed of a nanosized graphite sheet and linear gold chains and observed a large variation of conductance depending on the manner of connections between a graphite sheet and gold chains. With respect to the exponential law of conductance in nanosized graphite sheets with zigzag edges, we found an interesting feature on the transmission coefficient. The conductance in a series of zigzag-edge sheets is enhanced with an increase in size. Clearly, the localized electronic nature at the zigzag edges results in the reverse exponential law of conductance, in contrast to typical π-conjugated systems such as poly(acetylene) and poly(*para*-phenylene). To study how the existence of defects affects the conductance, we investigated graphite sheets that involve disordered zigzag edges, disordered armchair edges, and a hole. Defects at the zigzag edges tend to delocalize the π-electronic population over the graphite sheets, and therefore, there is no localized state that leads to significant quantum transport. On the other hand, defects at the armchair edges and existence of a hole are insensitive to the localization of π-electronic population.

Acknowledgment. K.Y. acknowledges the Ministry of Culture, Sports, Science and Technology of Japan (MEXT), Japan Society for the Promotion of Science, Japan Science and Technology Cooperation, the Murata Science Foundation, Kyushu University P & P "Green Chemistry", and "Nanotechnology Support Project" of MEXT for their support of this work. Computations were in part carried out at the Computer Center of the Institute for Molecular Science.

Appendix A. The Single Path Model (The CCNS Model)

Figure 9a shows a schematic representation of a molecular junction introduced by CCNS,[21] in which the tunneling current in the molecular junction is caused by interactions $\beta^T_{a\alpha}$ and $\beta^T_{\alpha' a'}$. In the CCNS model, conductance of the molecular junction is calculated from the Green's function $G_{aa'}$. The Dyson equation for $G_{aa'}$ is written as

$$G_{aa'} = G^{(0)}_{aa'} + G^{(0)}_{aa}\,\tau_{aa}G_{aa'} + G^{(0)}_{aa'}\,\tau_{a'a'}G_{a'a'} \qquad \text{(A1)}$$

To represent $G_{aa'}$ in terms of $G^{(0)}$'s and τ's only, we need the Dyson equation for $G_{a'a'}$, which is given as

$$G_{a'a'} = G^{(0)}_{a'a'} + G^{(0)}_{a'a'}\,\tau_{a'a'}G_{a'a'} + G^{(0)}_{a'a}\,\tau_{aa}G_{aa'} \qquad \text{(A2)}$$

When eq A2 is substituted in eq A1, we obtain

$$G_{aa'} = \frac{G^{(0)}_{aa'}}{(1 - G^{(0)}_{aa}\,\tau_{aa})(1 - G^{(0)}_{a'a'}\,\tau_{a'a'}) - G^{(0)}_{aa'}\,\tau_{aa}\,G^{(0)}_{a'a}\,\tau_{a'a'}} \qquad \text{(A3)}$$

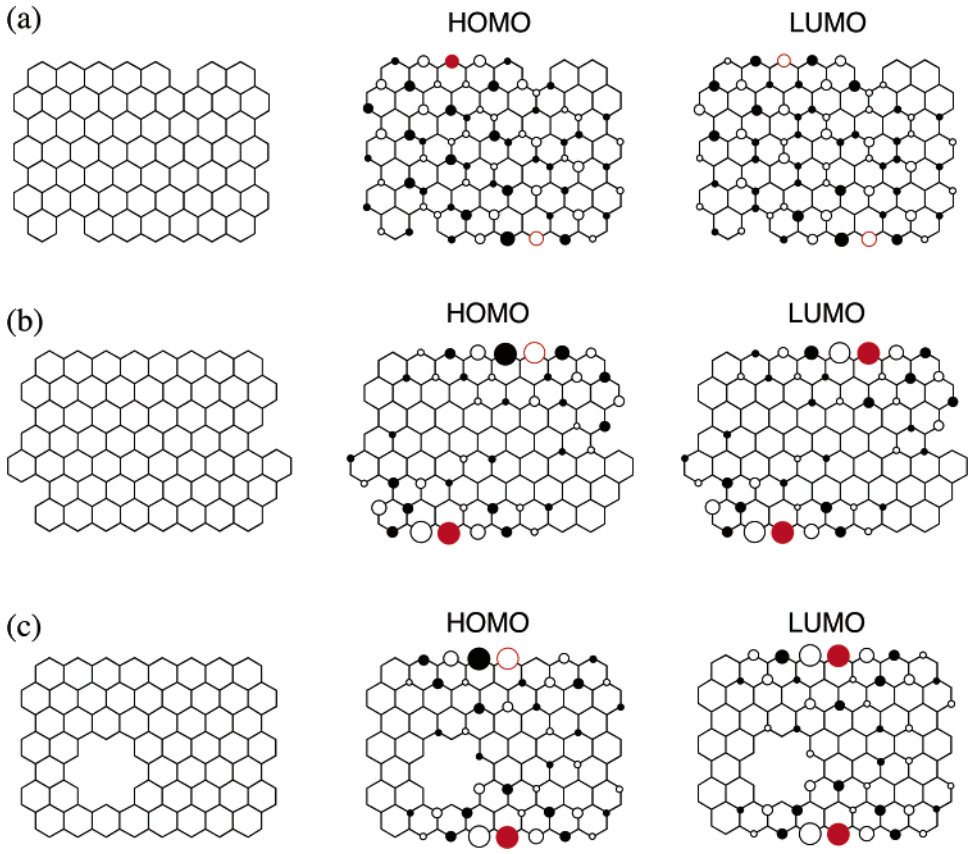

Figure 8. Graphite sheets with defects derived from R(8,7). These graphite sheets contain (a) disordered zigzag edges, (b) disordered armchair edges, and (c) a hole. The most efficient sites for quantum transport are drawn in the HOMOs and LUMOs with red circles.

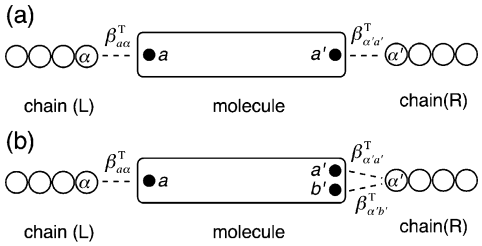

Figure 9. Schematic representation of molecular junctions with (a) single-path and (b) double-path interactions.

Double Path Model. To derive a general expression for Green's functions, we consider a double path model shown in Figure 9b, in which an interaction $\beta^{T}_{\alpha'b'}$ is added to the single path model. The Dyson equation for $G_{aa'}$ is written as

$$G_{aa'} = G^{(0)}_{aa'} + G^{(0)}_{aa}\,\tau_{aa}G_{aa'} + G^{(0)}_{aa'}\,\tau_{a'a'}G_{a'a'} + G^{(0)}_{ab'}\,\tau_{b'b'}G_{b'a'} + G^{(0)}_{aa'}\,\tau_{a'b'}G_{b'a'} + G^{(0)}_{ab'}\,\tau_{b'a'}G_{a'a'} \quad \text{(A4)}$$

in which the fourth, fifth, and sixth terms are newly added due to the interaction $\beta^{T}_{\alpha'b'}$. The Dyson equations for $G_{a'a'}$ and $G_{b'a'}$ are given as

$$G_{a'a'} = G^{(0)}_{a'a'} + G^{(0)}_{a'a}\,\tau_{aa}G_{aa'} + G^{(0)}_{a'a'}\,\tau_{a'a'}G_{a'a'} + G^{(0)}_{a'b'}\,\tau_{b'b'}G_{b'a'} + G^{(0)}_{a'a'}\,\tau_{a'b'}G_{b'a'} + G^{(0)}_{a'b'}\,\tau_{b'a'}G_{a'a'} \quad \text{(A5)}$$

and

$$G_{b'a'} = G^{(0)}_{b'a'} + G^{(0)}_{b'a}\,\tau_{aa}G_{aa'} + G^{(0)}_{b'a'}\,\tau_{a'a'}G_{a'a'} + G^{(0)}_{b'b'}\,\tau_{b'b'}G_{b'a'} + G^{(0)}_{b'a'}\,\tau_{a'b'}G_{b'a'} + G^{(0)}_{b'b'}\,\tau_{b'a'}G_{a'a'} \quad \text{(A6)}$$

respectively. Using eqs A5 and A6, we obtain the solution of eq A4 as

$$G_{aa'} = \frac{G^{(0)}_{aa'}(1 - G^{(0)}_{b'a'}\,\tau_{a'b'} - G^{(0)}_{b'b'}\,\tau_{b'b'}) + G^{(0)}_{ab'}(\tau_{b'a'}G^{(0)}_{a'a'} + \tau_{b'b'}G^{(0)}_{b'a'})}{D} \quad \text{(A7)}$$

where

$$\begin{aligned} D = {} & (1 - G^{(0)}_{aa}\,\tau_{aa})(1 - G^{(0)}_{a'a'}\,\tau_{a'a'} - G^{(0)}_{a'b'}\,\tau_{b'a'}) \times \\ & (1 - G^{(0)}_{b'a'}\,\tau_{a'b'} - G^{(0)}_{b'b'}\,\tau_{b'b'}) - (G^{(0)}_{a'a'}\,\tau_{a'b'} + G^{(0)}_{a'b'}\,\tau_{b'b'}) \times \\ & (G^{(0)}_{b'a'}\,\tau_{a'a'} + G^{(0)}_{b'b'}\,\tau_{b'a'})(1 - G^{(0)}_{aa}\,\tau_{aa}) - (G^{(0)}_{ab'}\,\tau_{b'b'} + G^{(0)}_{aa'}\tau_{a'b'}) \times \\ & G^{(0)}_{b'a}\,\tau_{aa}(1 - G^{(0)}_{a'a'}\,\tau_{a'a'} - G^{(0)}_{a'b'}\,\tau_{b'a'}) - (G^{(0)}_{aa'}\tau_{a'a'} + G^{(0)}_{ab'}\,\tau_{b'a'}) \times \\ & G^{(0)}_{a'a}\,\tau_{aa}(1 - G^{(0)}_{b'b'}\,\tau_{b'b'} - G^{(0)}_{a'b'}\,\tau_{a'b'}) - (G^{(0)}_{ab'}\,\tau_{b'b'} + G^{(0)}_{aa'}\tau_{a'b'}) \times \\ & (G^{(0)}_{b'a'}\,\tau_{a'a'} + G^{(0)}_{b'b'}\,\tau_{b'a'})\,G^{(0)}_{a'a}\,\tau_{aa} - (G^{(0)}_{aa'}\tau_{a'a'} + G^{(0)}_{ab'}\,\tau_{b'a'}) \times \\ & (G^{(0)}_{a'b'}\,\tau_{b'b'} + G^{(0)}_{a'a'}\,\tau_{a'b'})G^{(0)}_{b'a}\,\tau_{aa} \quad \text{(A8)} \end{aligned}$$

Assuming that the self-energy terms τ's are less than 1 eV, we can reasonably neglect higher terms of τ^3 in eq A8 and obtain the following expression:

$$G_{aa'} = \frac{G^{(0)}_{aa'}(1 - \sum_{k'=a'(\neq a')}^{b'}\sum_{l'=a'}^{b'} G^{(0)}_{k'l'}\,\tau_{l'k'}) + \sum_{m'=a'(\neq a')}^{b'}\sum_{n'=a'}^{b'} G^{(0)}_{am'}\,\tau_{m'n'}\,G^{(0)}_{n'a'}\,\tau}{D'} \quad \text{(A9)}$$

where

$$D' = (1 - G^{(0)}_{aa}\tau_{aa})\prod_{k'=a'}^{b'}(1 - \sum_{l'=a'}^{b'} G^{(0)}_{k'l'}\tau_{l'k'}) - \sum_{k''=a(<l'')}^{a'}\sum_{l''=a'}^{b'} \times (\dot{\sum_{p}} G^{(0)}_{k''p}\tau_{pl''})(\dot{\sum_{q}} G^{(0)}_{l''q}\tau_{qk''}) \quad \text{(A10)}$$

Here we adopted the same rules for k'', l'', and dotted Σ's given in the text. Including several interactions between the left side of a molecule and a gold chain as well as in the right side, we obtain the expression for Green's function of eq 4.

Appendix B. The PPP Hamiltonian

In the PPP method,[40] the off-diagonal elements of the Hamiltonian matrix are

$$H_{ij} = \sum_{i,j}\beta_{ij} - \frac{1}{2}P_{ij}\gamma_{ij} \quad \text{(B1)}$$

and the diagonal elements are

$$H_{ii} = \sum_{i} U_i + \frac{1}{2}P_{ii}\gamma_{ii} + \sum_{j\neq i}(P_{jj} - Z_j)\gamma_{ij} \quad \text{(B2)}$$

The parameters used in this model are as follows: U_i is the ionization energy of carbon ($U_{2p\pi} = -11.16$ eV),[41] and a transfer integral β_{ij} can be estimated with the Wolfsberg−Helmholz formula.[42] Z_j is the charge of the core to which the jth AO belongs, and **P** is the density matrix of π electrons. The one-center two-electron integral γ_{ii} is taken from the difference of the ionization energy and electron affinity for carbon ($\gamma_{2p\pi-2p\pi} = 11.13$ eV).[41] The two center integrals γ_{ij} can be obtained from the one-center integrals according to Pariser and Parr.[23]

References and Notes

(1) (a) Landauer, R. *IBM J. Res. Dev.* **1988**, *32*, 306. (b) Landauer, R. *Phys. Scr.* **1992**, *T42*, 110.

(2) Datta, S. *Electronic Transport in Mesoscopic Systems*; Cambridge University Press: Cambridge, 1995.

(3) (a) Samanta, M. P.; Tian, W.; Datta, S.; Henderson, J. I.; Kubiak, C. P. *Phys. Rev. B* **1996**, *53*, 7626. (b) Damle, P. S.; Ghosh, A. W.; Datta, S. *Phys. Rev. B* **2001**, *64*, 201403. (c) Paulsson, M.; Datta, S. *Phys. Rev. B* **2003**, *67*, 241403.

(4) Emberly, E. G.; Kirczenow, G. *Phys. Rev. B* **1998**, *58*, 10911.

(5) (a) Yaliraki, S. N.; Roitberg, A. E.; Gonzalez, C.; Mujica, V.; Ratner, M. A. *J. Chem. Phys.* **1999**, *111*, 6997. (b) Xue, Y.; Datta, S.; Ratner, M. A. *J. Chem. Phys.* **2001**, *115*, 4292.

(6) Lang, N. D.; Avouris, P. *Phys. Rev. B* **2001**, *64*, 125323.

(7) Derosa, P. A.; Seminario, J. M. *J. Phys. Chem. B* **2001**, *105*, 471.

(8) (a) Wang, C.-K.; Fu, Y.; Luo, Y. *Phys. Chem. Chem. Phys.* **2001**, *3*, 5017. (b) Luo, Y.; Wang, C.-K.; Fu, Y. *J. Chem. Phys.* **2002**, *117*, 10283. (c) Luo, Y.; Wang, C.-K.; Fu, Y. *Chem. Phys. Lett.* **2003**, *369*, 299.

(9) (a) Taylor, J.; Guo, H.; Wang, J. *Phys. Rev. B* **2001**, *63*, 121104. (b) Alavi, S.; Larade, B.; Taylor, J.; Guo, H.; Seideman, T. *Chem. Phys.* **2002**, *281*, 293.

(10) Palacios, J. J.; Pérez-Jiménez, A. J.; Louis, E. *Phys. Rev. B* **2001**, *64*, 115411.

(11) (a) Grossmann, F.; Gutiérrez, R.; Schmidt, R. *ChemPhysChem* **2002**, *3*, 650. (b) Gutiérrez, R.; Fagas, G.; Richter, K.; Grossmann, F.; Schmidt, R. *Europhys. Lett.* **2003**, *62*, 90.

(12) Tagami, K.; Tsukada, M.; Matsumoto, T.; Kawai, T. *Phys. Rev. B* **2003**, *67*, 245324.

(13) Hohenberg, P.; Kohn, W. *Phys. Rev.* **1964**, *136*, B864.

(14) Kohn, W.; Sham, L. J. *Phys. Rev.* **1965**, *140*, A1133.

(15) Xue, Y.; Datta, S.; Ratner, M. A. *Chem. Phys.* **2002**, *281*, 151.

(16) Damle, P.; Ghosh, A. W.; Datta, S. *Chem. Phys.* **2002**, *281*, 171.

(17) Brandbyge, M.; Mozos, J.-L.; Ordejón, P.; Taylor, J.; Stokbro, K. *Phys. Rev. B* **2002**, *65*, 165401.

(18) (a) Magoga, M.; Joachim, C. *Phys. Rev. B* **1997**, *56*, 4722. (b) Joachim, C.; Magoga, M. *Chem. Phys.* **2002**, *281*, 347. (c) Magoga, M.; Joachim, C. *Phys. Rev. B* **1998**, *57*, 1820.

(19) Quantum transport effects in nanosized graphite sheets are significantly enhanced when the following two conditions are satisfied: (I) The MO coefficients of two atoms connected with metallic leads are large in the highest occupied MO (HOMO) and the lowest unoccupied MO (LUMO), and (II) the product of MO coefficients on the two atoms in the HOMO is different in sign from that in the LUMO. Tada, T.; Yoshizawa, K. *ChemPhysChem* **2002**, *3*, 1035.

(20) Tada, T.; Yoshizawa, K. *J. Phys. Chem. B* **2003**, *107*, 8789.

(21) Caroli, C.; Combescot, R.; Nozieres, P.; Saint-James, D. *J. Phys. C: Solid State Phys.* **1971**, *4*, 916.

(22) (a) Becke, A. D. *Phys. Rev. A* **1988**, *38*, 3098. (b) Becke, A. D. *J. Chem. Phys.* **1993**, *98*, 5648. (c) Lee, C.; Yang, W.; Parr, R. G. *Phys. Rev. B* **1988**, *37*, 785. (d) Stephens, P. J.; Devlin, F. J.; Chabalowski, C. F.; Frisch, M. J. *J. Phys. Chem.* **1994**, *98*, 11623.

(23) (a) Pariser, R.; Parr, R. G. *J. Chem. Phys.* **1953**, *21*, 767. (b) Pople, J. A. *Trans. Faraday Soc.* **1953**, *49*, 1375.

(24) Kondo, Y.; Takayanagi, K. *Science* **2000**, *289*, 606.

(25) (a) Nilius, N.; Wallis, T. M.; Ho, W. *Science* **2002**, *297*, 1853. (b) Wallis, T.; Nilius, N.; Ho, W. *Phys. Rev. Lett.* **2002**, *89*, 236802.

(26) (a) Ditchfield, R.; Hehre, W. J.; Pople, J. A. *J. Chem. Phys.* **1971**, *54*, 724. (b) Hehre, W. J.; Ditchfield, R.; Pople, J. A. *J. Chem. Phys.* **1972**, *56*, 2257.

(27) Frisch, M. J.; Trucks, G. W.; Schlegel, H. B.; Scuseria, G. E.; Robb, M. A.; Cheeseman, J. R.; Zakrzewski, V. G.; Montgomery, J. A., Jr.; Stratmann, R. E.; Burant, J. C.; Dapprich, S.; Millam, J. M.; Daniels, A. D.; Kudin, K. N.; Strain, M. C.; Farkas, O.; Tomasi, J.; Barone, V.; Cossi, M.; Cammi, R.; Mennucci, B.; Pomelli, C.; Adamo, C.; Clifford, S.; Ochterski, J.; Petersson, G. A.; Ayala, P. Y.; Cui, Q.; Morokuma, K.; Malick, D. K.; Rabuck, A. D.; Raghavachari, K.; Foresman, J. B.; Cioslowski, J.; Ortiz, J. V.; Stefanov, B. B.; Liu, G.; Liashenko, A.; Piskorz, P.; Komaromi, I.; Gomperts, R.; Martin, R. L.; Fox, D. J.; Keith, T.; Al-Laham, M. A.; Peng, C. Y.; Nanayakkara, A.; Gonzalez, C.; Challacombe, M.; Gill, P. M. W.; Johnson, B. G.; Chen, W.; Wong, M. W.; Andres, J. L.; Head-Gordon, M.; Replogle, E. S.; Pople, J. A. *Gaussian 98*, revision x.x; Gaussian, Inc.: Pittsburgh, PA, 1998.

(28) The integral $\beta^{T}_{2p\pi-6s}$ was estimated from the extended Hückel method in the case where the interatomic distances between carbon and gold atoms are 3.36 Å, the van der Waals contact distance.

(29) Andrae, D.; Häuβermann, U.; Dolg, M.; Stoll, H.; Preuβ, H. *Theor. Chim. Acta* **1990**, *77*, 123.

(30) Dovesi, R.; Saunders: V. R.; Roetti, C.; Causà, M.; Harrison, N. M.; Orlando, R.; Aprà, E. *CRYSTAL 95 User's Manual*; Theoretical Chemistry Group: University of Torino, Torino, Italy, 1996.

(31) Pisani, C.; Dovesi, R.; Roetti, C. Hartree-Fock Ab Initio Treatmentof Crystalline Systems. In *Lecture Notes in Chemistry*; Berthier, G., et al., Eds.; Springer: Berlin, 1988; Vol. 48.

(32) *Quantum-Mechanical Ab initio Calculation of the Properties of Crystalline Materials*; Pisani, C., Ed.; Springer: Berlin, 1996.

(33) Broene, R. D.; Diederich, F. *Tetrahedron Lett.* **1991**, *32*, 5227.

(34) Wildöer, J. W. G.; Venema, L. C.; Rinzler, A. G.; Smalley, R. E.; Dekker: C. *Nature* **1998**, *391*, 59.

(35) (a) Xue, Y.; Datta, S. *Phys. Rev. Lett.* **1999**, *83*, 4844. (b) Anantram, M. P.; Datta, S.; Xue, Y. *Phys. Rev. B* **2000**, *61*, 14219.

(36) Molecular formulas are $C_{40}H_{16}$ for R(4, 3), $C_{56}H_{20}$ for R(6, 3), $C_{116}H_{28}$ for R(6, 7), $C_{148}H_{32}$ for R(8, 7), $C_{176}H_{36}$ for R(6, 11), and $C_{224}H_{40}$ for R(8, 11).

(37) For example, see: (a) Berresheim, A. J.; Müller, M.; Müllen, K. *Chem. Rev.* **1999**, *99*, 1747. (b) Boden, N.; Bushby, R. J.; Clements, J.; Movaghar, B. *J. Mater. Chem.* **1999**, *9*, 2081. (c) Keil, M.; Samorí, P.; dos Santos, D. A.; Kugler, T.; Stafström, S.; Brand, J. D.; Müllen, K.; Brédas, J. L.; Rabe, J. P.; Salaneck, W. R. *J. Phys. Chem. B* **2000**, *104*, 3967. (d) Meier, H. *Synthesis* **2002**, 1213. (e) Fischbach, I.; Pakula, T.; Minkin, P.; Fechtenkötter, A.; Müllen, K.; Spiess, H. W.; Saalwächter, K. *J. Phys. Chem. B* **2002**, *106*, 6408.

(38) Molecular formulas of R(8, 15) and R(8, 19) are $C_{300}H_{48}$ and $C_{376}H_{56}$, respectively.

(39) Geometry optimizations of R(8, 5) ($C_{110}H_{28}$) and R(8, 7) ($C_{148}H_{32}$) were carried out with the PM3 method. Stewart, J. J. P. *J. Comput. Chem.* **1989**, *10*, 209.

(40) Murrell, J. N.; Harget, A. J. *Semi-empirical self-consistent-field molecular orbital theory of molecules*; John Wiley & Sons Ltd: London, 1972.

(41) (a) Hinze, J.; Jaffe H. H. *J. Am. Chem. Soc.* **1962**, *84*, 540. (b) Dewar, M. J. S.; Morita , T. *J. Am. Chem. Soc.* **1969**, *91*, 796.

(42) Wolfsberg, M.; Helmholz, L. *J. Chem. Phys.* **1952**, *20*, 837.